J Solid State Electrochem (2010) 14:883–888
DOI 10.1007/s10008-009-0882-6

ORIGINAL PAPER

Preparation and electrochemical performance of $Li_3V_2(PO_4)_3$/C cathode material by spray-drying and carbothermal method

Feng Yu · Jingjie Zhang · Yanfeng Yang · Guangzhi Song

Received: 19 March 2009 / Revised: 27 May 2009 / Accepted: 6 June 2009 / Published online: 23 June 2009

Abstract Composite $Li_3V_2(PO_4)_3$/C cathode material can be synthesized by spray-drying and carbothermal method. The monoclinic-phase $Li_3V_2(PO_4)_3$/C was prepared with the process of double spray drying at 260 °C and subsequent heat treatment at 750 °C for 12 h. The results indicate that the $Li_3V_2(PO_4)_3$/C presents large reversible discharge capacity of 121.9 mA h g^{-1} and charge capacity of 131.8 mA h g^{-1} at the current density of *C/5*, good rate capability with 61.1 mA h g^{-1} at *20C*, and excellent capacity retention rate close to 100% at various current densities in the region of 3.0–4.3 V.

Keywords $Li_3V_2(PO_4)_3$/C · Cathode material · Electrochemical performance · Spray-drying and carbothermal method (SDCTM)

Introduction

Rechargeable lithium-ion batteries have a higher energy density than conventional lead acid, nickel–cadmium, and even nickel metal hydride batteries. They are the most promising candidates, which are needed urgently to be used for application such as electric vehicles and hybrid electric vehicles, to meet demands of modern technology and to revolutionize consumer electronics. However, the commercial layered $LiCoO_2$ material utilized as the positive electrode suffers from high cost and inferior safety concerns that necessitate careful electronic control of the cell [1–3]. The lithium transition metal phosphates (such as $LiFePO_4$ and $Li_3V_2(PO_4)_3$) have attracted extensive interest among researchers because these polyanionic compounds show numerous appealing features such as high theoretical capacity, acceptable operating voltage, good cycle life, low cost, and superior safety [4–9].

Rather than the olivine-phase $LiFePO_4$ with only one lithium extraction/insertion site, the monoclinic $Li_3V_2(PO_4)_3$ (NASICON framework structure) contains three independent lithium sites, which can overcome the electronic and lithium diffusion limitations, improve the rate of extraction/insertion and hence the power density of battery, and optimize electrochemical performance under high-current regimes [6, 7, 10]. The theoretical capacity can reach 132 mA h g^{-1} when two lithium ions in monoclinic $Li_3V_2(PO_4)_3$ are electrochemically extracted and reversibly reinserted in the voltage range of 3.0–4.3 V. While its theoretical capacity can reach 197 mA h g^{-1} in the voltage range of 3.0–4.8 V (all three lithium ions extracted and inserted) [11]. Furthermore, several voltage steps corresponding to two-phase transition of $Li_3V_2(PO_4)_3$ have more potentials than $LiFePO_4$ in applying to high-voltage equipment and determining the charge/discharge capacities according to the size of voltage. Recently, there have been many attempts to research rechargeable $Li_3V_2(PO_4)_3$ as a lithium cathode. The most common method of obtaining $Li_3V_2(PO_4)_3$ is solid-state techniques using hydrogen or carbon as reduction agents. However, the reaction takes place at relative high temperatures and long sintering time, where the size of the gained particles is in the micron range

F. Yu · J. Zhang (✉) · Y. Yang · G. Song
Technical Institute of Physics and Chemistry,
Chinese Academy of Sciences,
Beijing 100190, People's Republic of China
e-mail: jjzhang@mail.ipc.ac.cn

F. Yu
Graduate School of Chinese Academy of Sciences,
Beijing 100049, People's Republic of China
e-mail: yufeng05@mail.ipc.ac.cn

[7–9, 12–15]. The nanostructured $Li_3V_2(PO_4)_3$/C composite material is mostly carried out by sol-gel method [10, 11, 16–18], hydrothermal method [16], and rheological-phase reaction method [19]. Carbon coating is also considered to be the most effective way to improve the electrochemical performance of the cathode material.

Spray-drying technology is well known to be an attractive route to synthesize fine homogeneous and multicomponent powders. In comparison with the particles prepared by solid-state reaction, it is a tempting prospect to add a carbon source at the beginning of the synthesis where it will automatically be mixed into the materials by solution processes at a molecular size level. Moreover, this method exhibits superior performance including energy saving, cost effectiveness, continuous preparation, and environmental benignity [20, 21]. In this paper, we firstly report the preparation and electrochemical characteristic of homogeneous nanostructured $Li_3V_2(PO_4)_3$/C cathode material by spray-drying and carbothermal method (SDCTM). At the spray-drying step, the carbon source citric acid can be evenly distributed in the precursor solution and then uniformly distributed in the precursor. At the subsequent carbothermal reduction step, the carbon from citrate degradation and carbonization provides the special environment favorable for the reduction of pentavalent vanadium and the formation of the nanocrystalline composite $Li_3V_2(PO_4)_3$/C powders [10, 11, 16–19]. The obtained $Li_3V_2(PO_4)_3$/C powders possess a pure well-crystallized phase, even carbon coating and uniform particle morphology with nanosized distribution for achieving good discharge capacities, rate capabilities, and cycle performances. The electrochemical performance of the prepared $Li_3V_2(PO_4)_3$/C cathode powders was examined with capacity retention studies performed with various rates in the voltage of 3.0–4.3 V and 3.0–4.8 V.

Experiment

Amounts of LiOH(AR), NH_4VO_3(AR), H_3PO_4(AR), and citric acid(AR) were dissolved in distilled water in the stoichiometric ratio: $n_{Li}/n_V/n_P/n_{acid}$=3:2:3:1. The aqueous solution was made to prepare a homogeneous emulsion (solid content 20 wt.%). The emulsion was spray-dried in a spray dryer unit at a rate of 15 mL/min with inlet and outlet temperatures kept at 260 °C and 130 °C. Its rotation speed is 18,000 revolutions. The obtained power was dissolved in distilled water to prepare a solution (solid content 20 wt.%) and spray-dried again. Then, the obtained precursor was burned out at 120 °C for 5 h in an air-limited box furnace. Finally, carbothermal reduction of spray-dried precursor was performed in a tube furnace using a graphite crucible, heated at 10 °C/min in flowing argon atmosphere (100 mL/min) up to 750 °C and held for 12 h.

The crystalline structure of the prepared $Li_3V_2(PO_4)_3$/C powders was studied by X-ray diffractometer (D/max 2200 PC, Japan), with CuKα radiation at 40 kV, 40 mA, step size of 0.02°, and a count time of 0.6 s per step between 2θ= 10–80°. The scanning electron microscopy (SEM) images and energy-dispersive X-ray (EDX) were obtained using a Hitachi S-4300 microscope and EMAX Horiba, respectively. Transmission electron microscope (TEM; JEM 200CX, Japan) was also used to analyze the morphology of the prepared powders.

For fabrication of the working electrodes, the prepared powders were mixed with acetylene black and polyvinylidene fluoride in weight ratio of 80:10:10 in *N*-methyl-2 pyrrolidinone. The obtained slurry was coated onto Al foil and dried at 80 °C for 4 h. Then, the dried tape was punched into round plates with a diameter of 10.0 mm as cathode electrodes (5–8 mg cm^{-2} loading). The electrodes were dried again at 120 °C for 5 h in a vacuum prior to use. Finally, the prepared cathodes and Celgard2400 separator (diameter of 16.0 mm) were placed into an argon atmosphere filled glove box (H_2O and O_2<1 ppm) and assembled into a coin cell (CR2032) with lithium anode, electrolyte of 1 M $LiPF_6$ in EC–DEC–DMC (1:1:1 vol.%), and the other components of the coin-type cell. The cells were charged and discharged at various current densities (current density of 132 mA g^{-1} is equivalent to *1C* rate) on a battery tester in the voltage of 3.0–4.3 or 3.0–4.8 V at room temperature. Meanwhile, the cells were retained 10 min at 4.3 or 4.8 V in charging.

Results and discussion

The X-ray diffraction pattern of $Li_3V_2(PO_4)_3$/C powders prepared at 750 °C for 12 h is shown in Fig. 1. The profiles of the reflection peaks are quite narrow and symmetric. The diffraction lines can be attributed to the monoclinic-phase

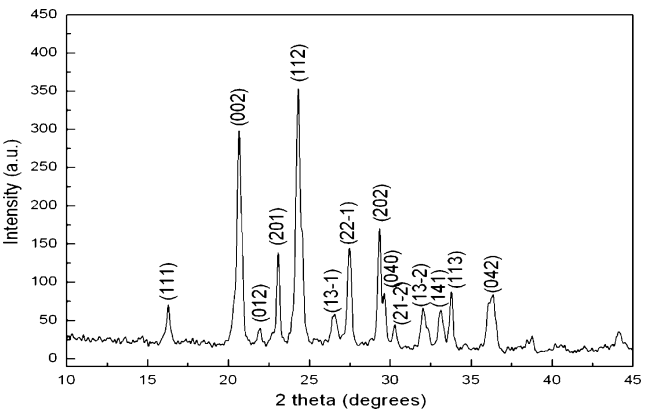

Fig. 1 X-ray diffraction pattern of $Li_3V_2(PO_4)_3$/C prepared at 750 °C for 12 h

Table 1 Comparison of lattice parameters of $Li_3V_2(PO_4)_3$/C samples

Samples	*a* axis (nm)	*b* axis (nm)	*c* axis (nm)	β (°)	Cell volume (nm^3)
$Li_3V_2(PO_4)_3$/C	0.8609	1.2062	0.8582	89.92	0.8913
Huang et al. [10]	0.8620	1.2055	0.8609	89.92	0.8992
Chen et al. [11]	0.8620	1.2061	0.8609	90.57	0.8950

$Li_3V_2(PO_4)_3$ without any impurity phase. It is in good agreement with the pattern of the monoclinic $Li_3Fe_2(PO_4)_3$ (PDF#47-0107). Otherwise, the carbon is not detected because the residual carbon is amorphous. A space group of $P2_{1/n}$ was selected as the refinement model. The absolute lattice parameters for the sample are as follows: a= 0.8609 nm, b=1.2062 nm, c=0.8582 nm, β=89.92°, and the cell volume exhibits V=0.8913 nm^3, similar to the previous report (Table 1). Moreover, the mean crystallite size of the $Li_3V_2(PO_4)$ is 42 nm (Debye–Scherrer equation), which is much smaller than those prepared by conventional solid-state method. Thereby, a pure homogeneous and well-crystallized $Li_3V_2(PO_4)_3$/C material is indicated.

SEM was used to analyze the particle morphology and size of $Li_3V_2(PO_4)_3$/C powders, which are shown in Fig. 2a. In the SEM image, the $Li_3V_2(PO_4)_3$/C particles show good uniformity and have no coalescence. In order to further clarify the microstructure of the sample and check carbon distribution in the powders, TEM investigation was also conducted and the result is displayed in Fig. 2b. In the TEM image, it can be seen that the $Li_3V_2(PO_4)_3$/C particles have a size of about 200 nm. The light gray represents the formed carbon, while the black region originates from $Li_3V_2(PO_4)_3$. The surface of $Li_3V_2(PO_4)_3$ coated with the formed carbon, which can impede the grain growth of the $Li_3V_2(PO_4)$, and enhance the electronic conductivity of the cathode materials. Figure 2c shows a representative EDX spectrum of $Li_3V_2(PO_4)_3$/C composite and Table 2 shows the analysis results of main element content. It can be obtained that the carbon content is 7.64 wt.%. This indicates that citric acid is decomposed into carbon during the calcination, and residual carbon homogeneously exists in $Li_3V_2(PO_4)_3$. Moreover, this microstructure will facilitate

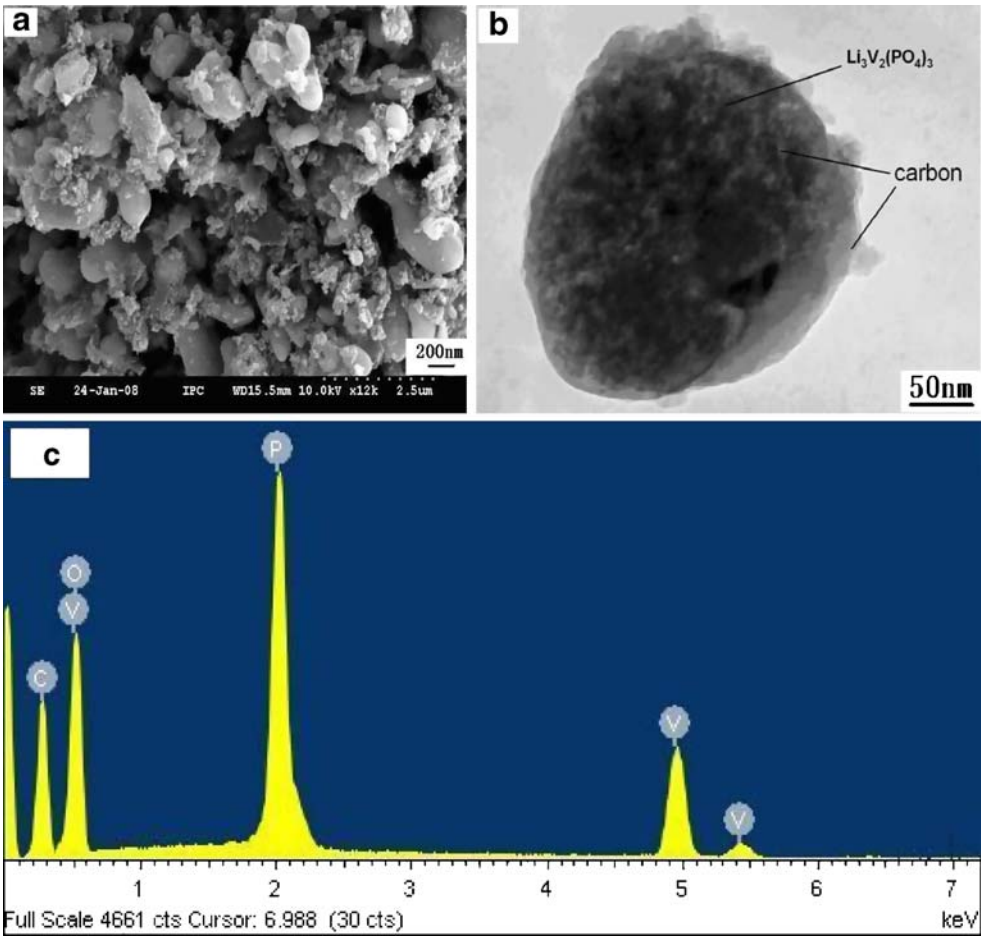

Fig. 2 **a** Typical scanning electron microscopy image, **b** transmission electron microscopy image, and **c** energy-dispersive X-ray spectrum of $Li_3V_2(PO_4)_3$/C composite

Table 2 Analysis results of main element content of $Li_3V_2(PO_4)_3$/C by EDX

Element	Weight (%)	Atomic (%)
C	7.64	13.57
O	45.68	60.91
P	22.15	15.25
V	24.53	10.27

the lithium-ion diffusion during insertion/extraction processes and lead to the reduction of the cell resistance.

Figure 3 shows selected galvanostatic charge–discharge profiles and its cyclic performance of $Li_3V_2(PO_4)_3$/C at room temperature cycled in the voltage of 3.0–4.3 V and 3.0–4.8 V at a current density of 26 mA g^{-1}. From Fig. 3a, the profiles all exhibit three typical flat discharge plateaus close to 3.56, 3.65, and 4.05 V and the corresponding three charge ones close to 3.61, 3.68,and 4.10 V, which is corresponding to three compositional transitions between different phases of $Li_xV_2(PO_4)_3$, that is x=3.0 (1), x=2.5 (2), x=2.0 (3), and x=1.0 (4). The above reactions involved may be summarized as:

(1)→(2): $Li_3V_2(PO_4)_3 \rightarrow Li_{2.5}V_2(PO_4)_3 + 0.5Li^+ + 0.5e^-$ (charge)

(2)→(3): $Li_{2.5}V_2(PO_4)_3 \rightarrow Li_2V_2(PO_4)_3 + 0.5Li^+ + 0.5e^-$ (charge)

(3)→(4): $Li_2V_2(PO_4)_3 \rightarrow LiV_2(PO_4)_3 + Li^+ + e^-$ (charge)

It is also found that the electrode displays a reversible discharge capacity of 121.9 mA h g^{-1} and charge capacity of 131.8 mA h g^{-1}. Thus, the sample shows the high coulombic efficiency of 92.5%. In addition, the charge and discharge profiles almost unchanged and hardly polarized from the fifth cycle. The charge and discharge capacity values both exhibit good reversible capacity with a capacity retention rate of about 100% upon cycling and after 30 cycles, as shown in Fig. 3b. It is noted that $Li_3V_2(PO_4)_3$/C material has good cyclic capacity and electrochemical stability in the voltage range of 3.0–4.3 V.

Figure 3c shows the charge–discharge profiles and the corresponding cyclic performance of $Li_3V_2(PO_4)_3$/C cycled in the voltage of 3.0–4.8 V. It can be seen that the sample has clear charge plateaus in the first and 30th cycles. The sample exhibits the fourth charge flat plateaus close to 4.56 V, which reaction may be summarized as: (4)→(5): $LiV_2(PO_4)_3 \rightarrow V_2(PO_4)_3 + Li^+ + e^-$ (charge). The initial discharge-specific capacity of $Li_3V_2(PO_4)_3$/C presents initial discharge capacity of 172.4 mA h g^{-1}. Subsequently, fading of discharge capacity is observed after 30cyles and the discharge capacity remains 147.7 mA h g^{-1}, which is

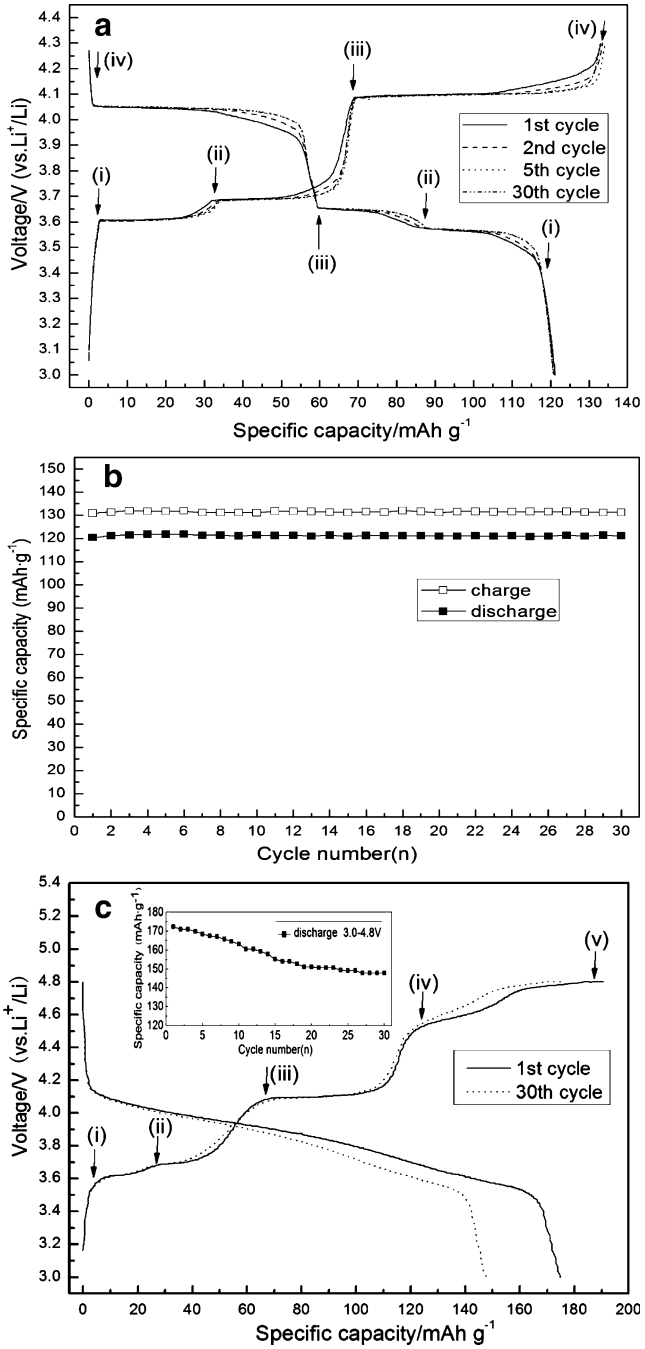

Fig. 3 **a** Galvanostatic charge–discharge profiles of $Li_3V_2(PO_4)_3$/C at room temperature cycled in the voltage of 3.0–4.3 V at a current density of 26 mA g^{-1} (*C/5* rate). **b** The corresponding variation of charge and discharge capacities versus cycle number. **c** The charge–discharge profiles of $Li_3V_2(PO_4)_3$/C cycled in the voltage of 3.0–4.8 V at a current density of 26 mA g^{-1} and the corresponding cyclic performance (*insert*)

85.7% of the initial discharge capacity. It can be seen that there are no obvious discharge flat plateaus. Since the $Li_3V_2(PO_4)_3$/C particles contact with the electrolyte directly, the solid electrolyte interface (SEI) passivation layer will be formed in the first cycle. The SEI layer maintains steady

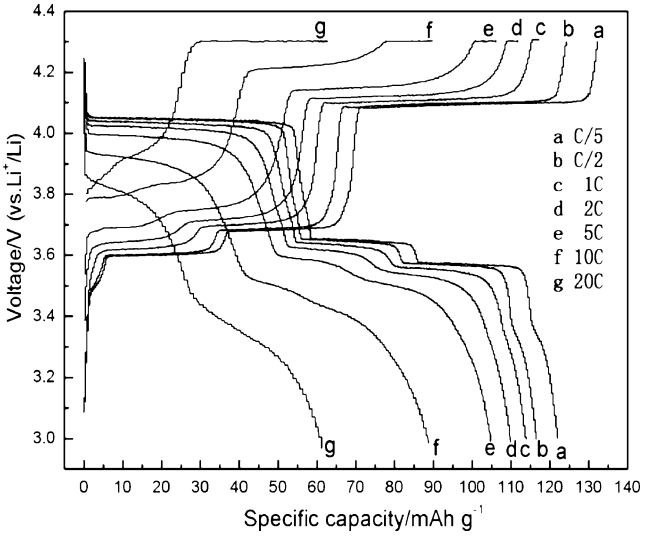

Fig. 4 Charge and discharge curves of $Li_3V_2(PO_4)_3$/C cathode materials at various rates. The discharge rates are the same as the charge rates separately in cycles

thickness and at least a high conductivity in subsequent cycles [22, 23]. Moreover, oxygen atoms are not easily separated from the P–O bands in this polyanion structure (PO_4^{3-}). In $Li_3V_2(PO_4)_3$ structure, each plateau corresponds to a two-phase transition involving the reorganization of electrons and Li ions within the lattice. The energies of structures spanning the phase transition are governed by the site potential of the Li^+ ion and their interaction with the V^{n+} ions in the lattice. Extracting the third lithium needs higher energy and irreversibility exists during charge–discharge, mainly leading to a performance deterioration during cycling [9, 18, 24].

The initial charge–discharge curves of $Li_3V_2(PO_4)_3$/C with various rates are shown in Fig. 4. It can be seen that the electrode presents lower discharge voltage and smaller reversible capacity at relatively higher rate, resulting from the rise of electrode polarization, which would increase by cycling the cell with high *C* rate and thus the specific capacity within a given potential window would decrease. However, electrode still delivers discharge capacities of 104.6 and 88.2 mA h g^{-1} at *5C* and *10C* rate, respectively, which confirm excellent rate capabilities with 86.1% and 72.5% of the maximum capacity (121.9 mA h g^{-1} at *C/5*) shown in Fig. 5. Even at a rate as high as *20C*, a reversible capacity of 61.1 mA h g^{-1} can be achieved. The good rate capability may be due to its excellent properties of Li^+ diffusion rate across NASICON structure such that $Li_3V_2(PO_4)_3$/C shows high specific capacity as it is discharged with higher *C* rates. The small observed voltage polarization also suggests that the $Li_3V_2(PO_4)_3$/C electrode should have high electrochemical reversibility.

The results of $Li_3V_2(PO_4)_3$/C cycling at various rates are presented in Fig. 6, which shows the voltage profiles for several cycles at room temperature. The specific discharge capacity decreases with increasing charge–discharge rate and reduces from 121.9 mA h g^{-1} at *C/5* rate to 61.1 mA h g^{-1} at *20C* rate because lithium diffusion and electronic conduction are limited. On the other hand, when the lower current density was applied, the electrode was able to retrieve its capacity, which confirms nearly 100% of the starting discharge capability. This retention of $Li_3V_2(PO_4)_3$/C on extended cycling shows that the $Li_3V_2(PO_4)_3$/C possesses an excellent rate capability and good cycle life. It could be attributed to the relative invariance of monoclinic

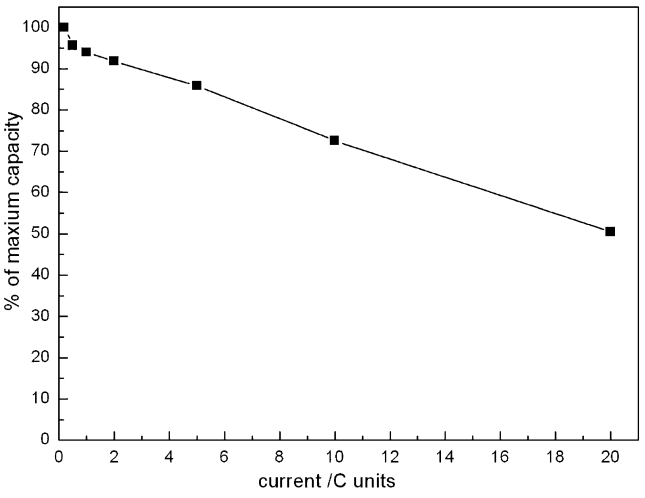

Fig. 5 Variation of discharge capacity as a function of rate cycled in the voltage of 3.0–4.3 V, expressed in terms of percentage of the maximum capacity obtained at low rate, for the $Li_3V_2(PO_4)_3$/C cathode at room temperature

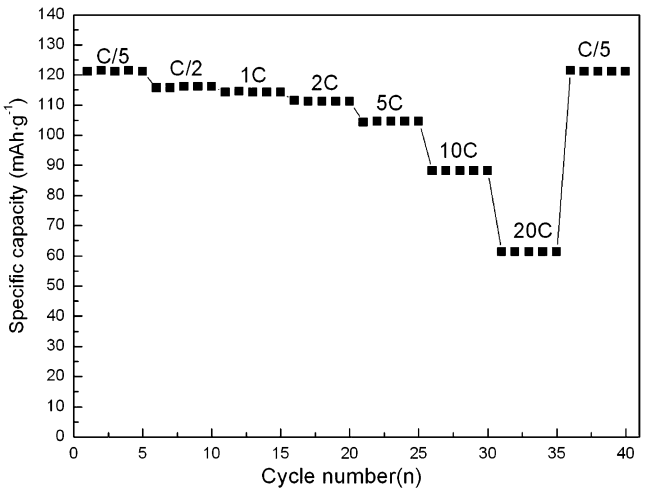

Fig. 6 Reversible capacities during continuous cycling at various discharge rates. The discharge rates are the same as the charge rates separately in cycles

$Li_3V_2(PO_4)_3$ host framework and highly uniform distribution of carbon in the $Li_3V_2(PO_4)_3$ particles.

Conclusion

The homogeneous monoclinic $Li_3V_2(PO_4)_3$/C particles have been successfully prepared by SDCTM using citric acid as both a chelating agent and carbon source. The $Li_3V_2(PO_4)_3$/C composite with an average size of about 200 nm presents large reversible capacity, good rate capability, and excellent cyclic stability in the region of 3.0–4.3 V. The composite $Li_3V_2(PO_4)_3$/C powder exhibits polarization as it is discharged with higher *C* rates but still displays stable discharge capacity cycle performance. Even at *20C* rate, a reversible discharge capacity of 61.1 mA h g^{-1} can be achieved. It almost displays all the electrochemical advantages of $Li_3V_2(PO_4)_3$/C material.

References

1. Scrosati B (1995) Nature 373:557
2. Whittingham MS (2004) Chem Rev 104:4271
3. Grey CP, Dupre N (2004) Chem Rev 104:4493
4. Padhi AK, Nanjundaswamy KS, Goodenough JB (1997) J Electrochem Soc 144:1188
5. Padhi AK, Nanjundaswamy KS, Masquelier C, Goodenough JB (1997) J Electrochem Soc 144:2581
6. Nanjundaswamy KS, Padhi AK, Goodenough JB, Okada S, Ohtsuka H, Arai H, Yamaki J (1996) Solid State Ionics 92:1
7. Gaubicher J, Wurm C, Goward G, Masquelier C, Nazar L (2000) Chem Mater 12:3240
8. Saidi MY, Barker J, Huang H, Swoyer JL, Adamson G (2003) J Power Sources 119–121:266
9. Yin SC, Grondey H, Strobel P, Anne M, Nazar LF (2003) J Am Chem Soc 125:10402
10. Huang H, Yin SC, Kerr T, Taylor N, Nazar LF (2002) Adv Mater 14:1525
11. Chen QQ, Wang JM, Tang Z, He WC, Shao HB, Zhang JQ (2007) Electrochim Acta 52:5251
12. Barker J, Saidi MY, Swoyer JL (2003) J Electrochem Soc 150: A684
13. Liu SQ, Li SC, Tang LX, Huang KL (2006) Chin J Inorg Chem 22:645
14. Fu P, Zhao YM, Dong YZ, An XN, Shen GP (2006) J Power Sources 162:651
15. Ren MM, Zhou Z, Li YZ, Gao XP, Yan J (2006) J Power Sources 162:1357
16. Ren MM, Zhang Z, Gao XP, Peng WX, Wei JP (2008) J Phys Chem C 112:5689
17. Li YZ, Zhou Z, Ren MM, Gao XP, Yan J (2006) Electrochim Acta 51:6498
18. Li YZ, Zhou Z, Gao XP, Yan J (2007) Electrochim Acta 52:4922
19. Chang CX, Xiang JF, Shi XX, Han XY, Yuan LJ, Sun JT (2008) Electrochim Acta 53:2232
20. Ju SH, Kang YC (2008) Mater Chem Phys 107:328
21. Wu HM, Tu JP, Chen XT, Shi DQ, Zhao XB, Gao GS (2006) Electrochim Acta 51:4148
22. Reddy MV, Pecquenard B, Vinatier P, Levasseur A (2007) Electrochem Commun 9:409
23. Striebel K, Shim J, Sierra A, Yang H, Song XY, Kostecki R, Mccarthy K (2005) J Power Sources 146:33
24. Yin SC, Grondey H, Strobel P, Huang H, Nazar LF (2003) J Am Chem Soc 125:326